The Astrophysical Journal, 746:13 (9pp), 2012 February 10 doi:10.1088/0004-637X/746/1/13

SDO/AIA OBSERVATIONS OF SECONDARY WAVES GENERATED BY INTERACTION OF THE 2011 JUNE 7 GLOBAL EUV WAVE WITH SOLAR CORONAL STRUCTURES

Ting Li[1], Jun Zhang[1], Shuhong Yang[1], and Wei Liu[2,3]
[1] Key Laboratory of Solar Activity, National Astronomical Observatories, Chinese Academy of Sciences, Beijing 100012, China; liting@nao.cas.cn; zjun@nao.cas.cn; shuhongyang@nao.cas.cn
[2] Lockheed Martin Solar and Astrophysics Laboratory, Department ADBS, Building 252, 3251 Hanover Street, Palo Alto, CA 94304, USA
[3] W. W. Hansen Experimental Physics Laboratory, Stanford University, Stanford, CA 94305, USA
Received 2011 August 27; accepted 2011 November 8; published 2012 January 19

ABSTRACT

We present *Solar Dynamics Observatory*/Atmospheric Imaging Assembly observations of the interaction of a global EUV wave on 2011 June 7 with active regions (ARs), coronal holes (CHs), and coronal bright structures. The primary global wave has a three-dimensional dome shape, with propagation speeds ranging from 430 to 780 km s^{-1} in different directions. The primary coronal wave runs in front of the expanding loops involved in the coronal mass ejection (CME) and its propagation speeds are approximately constant within 10–20 minutes. Upon arrival at an AR on its path, the primary EUV wave apparently disappears and a secondary wave rapidly reemerges within 75 Mm of the AR boundary at a similar speed. When the EUV wave encounters a coronal bright structure, an additional wave front appears there and propagates in front of it at a velocity nearly a factor of two faster. Reflected waves from a polar CH and a coronal bright structure are observed and propagate fractionally slower than the primary waves. Some of these phenomena can be equally explained by either a wave or a non-wave model alone. However, taken together, these observations provide new evidence for the multitudes of global EUV waves, in which a true MHD fast-mode wave or shock propagates in front of an expanding CME bubble.

Key words: Sun: activity – Sun: corona – Sun: coronal mass ejections (CMEs) – Sun: flares

Online-only material: animations, color figures

1. INTRODUCTION

Propagating global disturbances in the solar corona were first detected by the *Solar and Heliospheric Observatory* Extreme-ultraviolet Imaging Telescope (EIT; Delaboudinière et al. 1995; Moses et al. 1997; Thompson et al. 1998) and have since then been commonly called "EIT waves." However, there has been no satisfactory explanation about the nature of such disturbances. Many authors, such as Wang (2000), Warmuth et al. (2001), and Patsourakos & Vourlidas (2009), proposed that they are truly fast-mode magnetohydrodynamic (MHD) waves, while others (Delannée 2000; Chen et al. 2002; Attrill et al. 2007a, 2007b; Chen & Wu 2011; Schrijver et al. 2011) suggested they are apparent waves related to the opening and restructuring of magnetic field lines caused by a coronal mass ejection (CME). A combination of both true wave and non-wave mechanisms was then proposed to reconcile these disparate models (Zhukov & Auchère 2004; Cohen et al. 2009; Liu et al. 2010; Downs et al. 2011). For recent reviews, we refer to Vršnak & Cliver (2008), Wills-Davey & Attrill (2009), Gallagher & Long (2011), and Zhukov (2011).

Global coronal waves have been observed to interact with various coronal structures (Thompson et al. 1998, 1999; Delannée & Aulanier 1999; Wills-Davey & Thompson 1999; Veronig et al. 2006). They tend to avoid strong magnetic fields in active regions (ARs), stop at or partially penetrate into the boundaries of coronal holes (CHs), and stop near a separatrix between ARs. Stopping at CHs was confirmed by MHD simulations (Wang 2000; Wu et al. 2001). In addition, Ofman & Thompson (2002) found strong reflection and refraction of the primary wave from an AR, as well as secondary waves generated by the dynamic distortion of the AR magnetic field. Due to EIT's low cadence (12–15 minutes) and *TRACE*'s small field of view, it was difficult to test observationally such numerical simulations. This situation was partly alleviated with the launch of the *Solar-Terrestrial Relations Observatory* (*STEREO*; Kaiser et al. 2008) Extreme-Ultraviolet Imagers (EUVI; see Wuelser et al. 2004). It detected the first example of reflection and refraction of coronal waves at CH boundaries (Gopalswamy et al. 2009), which were recently numerically reproduced (Schmidt & Ofman 2010). However, *STEREO*'s improved, yet relatively low, cadence of 2.5 minutes left room for potential ambiguity and led to debates about the validity of this result (Attrill 2010).

The new Atmospheric Imaging Assembly (AIA; Lemen et al. 2011) on board the *Solar Dynamics Observatory* (*SDO*; Schwer et al. 2002) takes full-disk images in 10 (E)UV channels at 1.″5 resolution and high cadence of 12 s. It thus offers opportunities to elucidate previous ambiguities about the interaction of a global EUV wave with ARs and CHs. We report here such an example observed by AIA in unprecedented detail.

2. OBSERVATIONS AND DATA ANALYSIS

On 2011 June 7, *SDO*/AIA observed a spectacular solar eruptive event occurring in NOAA AR 11226 (S22W55). It involved an M2.5 flare, a filament eruption, a CME, and a global coronal EUV wave (Figure 1). Among the 10 wavelengths of AIA, the 193, 171, 211, and 335 Å channels clearly show the global EUV wave that has a dome-like shape (see also the wave on 2010 January 17 in Veronig et al. 2010) and we focus on these channels in this study. The wave signature is similar in the three hot channels, 193, 211, and 335 Å, but different in the cooler 171 Å channel. The four channels correspond to different temperatures: 193 Å (Fe XII) at 1.5 MK (with a hot contribution of Fe XXIV at 20 MK and cooler O V at 0.2 MK), 171 Å (Fe IX) at 0.6 MK, 211 Å (Fe XIV) at 2.0 MK, and 335 Å (Fe XVI) at 2.5 MK (O'Dwyer et al. 2010; Boerner et al. 2011).

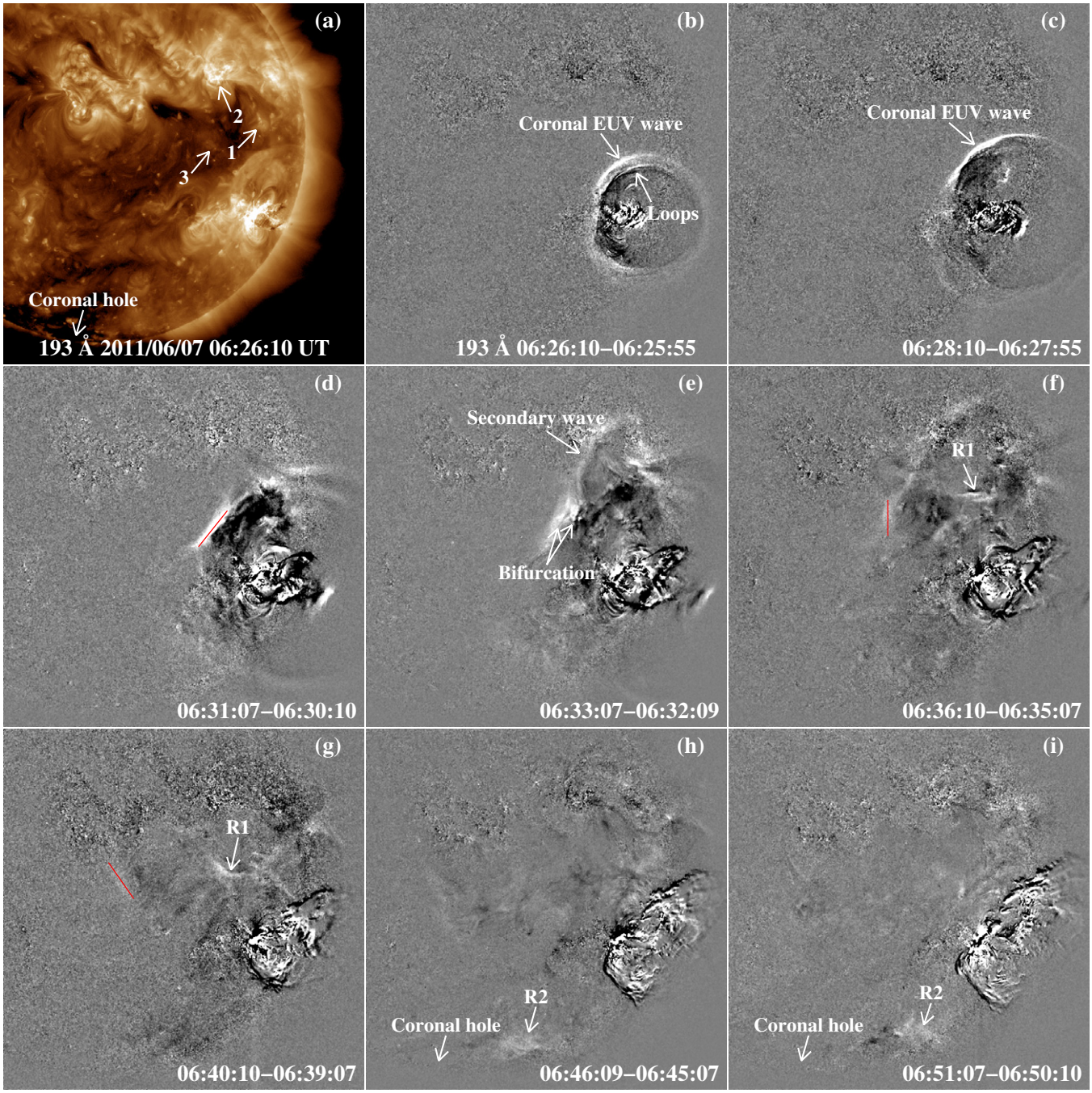

Figure 1. *SDO*/AIA 193 Å image (panel (a), see Animation 1) and running difference images (panels (b)–(i), see Animation 2) showing the evolution of the global coronal EUV wave on 2011 June 7. Arrows "1" and "3" in panel (a) point to two coronal bright structures hit by the coronal wave, and "2" denotes AR 11228. Red lines in panels (d), (f), and (g) represent the leading edges, indicating the deflection of the wave. "R1" and "R2" denote the reflected waves from the coronal bright structure "1" and from the southern polar CH, respectively.

(Animations and a color version of this figure are available in the online journal.)

The coronal wave was also observed by the EUVI on board *STEREO A* that was 95° ahead of the Earth (Figure 6(c)). EUVI observes the chromosphere and corona in four spectral channels (304 Å, 171 Å, 195 Å, and 284 Å) out to 1.7 $R_{\rm sun}$ with a pixel size of 1.″6.

Here, we use a semi-automatic method (see Podladchikova & Berghmans 2005; Liu et al. 2010) to obtain stack plots from 10° wide sectors on the solar surface ("A" and "C"–"G," Figure 2). Each data point in stack plots is the average of the pixels within a sector along a circular arc at the same distance from the eruption center (S22W55 for Sectors "A," "F," and "G") or the initiation site of secondary waves (N8W50 for Sectors "C"–"E").

3. RESULTS

3.1. Erupting Loops and Primary Global Coronal EUV Wave

At 193 Å, a series of erupting loops started to expand at 06:20:00 UT (Figures 3(b) and 5(a); Animation 2). They appear as bright stripes with increasing slopes. A parabolic fit indicates an acceleration of 86 m s^{-2} and a final velocity of 280 km s^{-1}.

At 06:24:33 UT, the global coronal EUV wave initiated in front of the erupting loops (Figures 1(b) and (c); see Animations 1 and 2). Seen from the stack plots (Figures 3(b) and 5(a)), the spatial separation between the coronal wave and

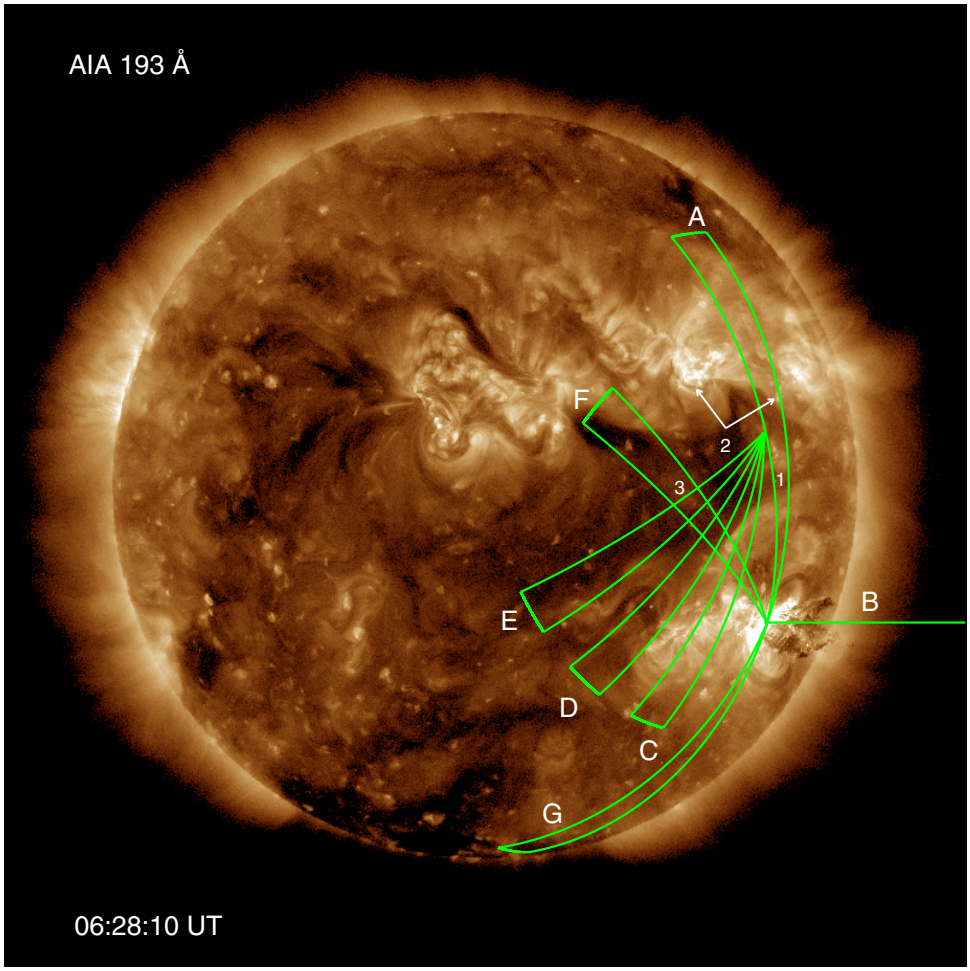

Figure 2. *SDO* /AIA 193 Å full-disk image showing six 10° wide sectors ("A" and "C"–"G") and slice "B," which are used to obtain the stack plots shown in Figures 3–5. "1" and "3" denote two coronal bright structures hit by the coronal wave, and "2" represents loop brightenings of AR 11228 (see Figures 3(d) and (e)).
(A color version of this figure is available in the online journal.)

the expanding loops indicates that the former propagates in front of the latter. In Sectors "A" and "F," the velocities of the wave are, respectively, 510 and 430 km s^{-1}, and remain constant over the propagation up to 350 Mm. The 211 and 335 Å observations in Sector "A" are similar to those of 193 Å (Figures 3(d) and (e)). However, the wave appears different at cooler 171 Å (Figure 3(c)). A group of small-scale coronal loops are impacted by the coronal wave and expand with a speed of 130 km s^{-1}. The expansion lasts about 3 minutes and then the loops contract to their initial state. This is a possible indicator of loop oscillations triggered by the passage of the EUV wave.

We also investigate the vertical propagation of the wave dome using a straight slice ("B"; Figures 2 and 3(g)). The initial expansion of the loops is evident in the stack plot. Then, it faded away with height due to the steep radial intensity gradient. The onset of the wave in this direction coincides with that of the lateral wave. The upward expansion of the dome has a uniform velocity of 730 km s^{-1} projected onto the sky plane within the AIA field of view, which is 1.5 times as fast as its lateral expansion to the north, but comparable to that of its lateral expansion toward the south. Note that the erupting filament material is much slower with a large velocity range from 80 km s^{-1} to 400 km s^{-1}, qualitatively similar to those of coronal jets (e.g., Liu et al. 2009, their Figure 2(a)). The wave signal along slice "B" is very weak at 171 Å (Figure 3(h)) and not observed at 335 Å (Figure 3(j)).

3.2. Secondary Wave Over AR 11228

At 06:30:19 UT, the dome-shaped wave encountered a coronal bright structure (denoted by "1" in Figure 1(a)) and the circular wave front was deformed (Figure 1(d)). Seen from the stack plot of Sector "A" (Figures 3(b)–(e)), the intensity of the coronal wave decreased rapidly after it passed through the coronal bright structure, with an increased velocity of 1340 km s^{-1} (Figure 3(b)).

About 2 minutes later, the weak wave arrived at the boundary of AR 11228 and apparently stopped there (denoted by "2" in Figure 2). Almost simultaneously, a secondary wave appeared about 75 Mm into the boundary, which is 506 Mm from the eruption center (Figures 1(e) and 3(b)–(e); see Animation 2). This wave lasted 7 minutes and the velocity decreased from 500 km s^{-1} to 250 km s^{-1} at 06:39:07 UT. The secondary wave is different from the primary wave in shape and kinematics. The former shows a clear deceleration, while the latter has a uniform velocity during the majority of its lifetime. At 211 and 335 Å, loop brightening in AR 11228 is observed from 06:32 UT (Figures 3(d) and (e)).

3.3. Reflected Waves from Bright Structures and a Polar CH

A reflected wave from the coronal bright structure "1" (Figures 1(a) and 2; see Animation 2) was observed between 06:33:46 UT and 06:42:10 UT ("R1" in Figures 1(f) and (g);

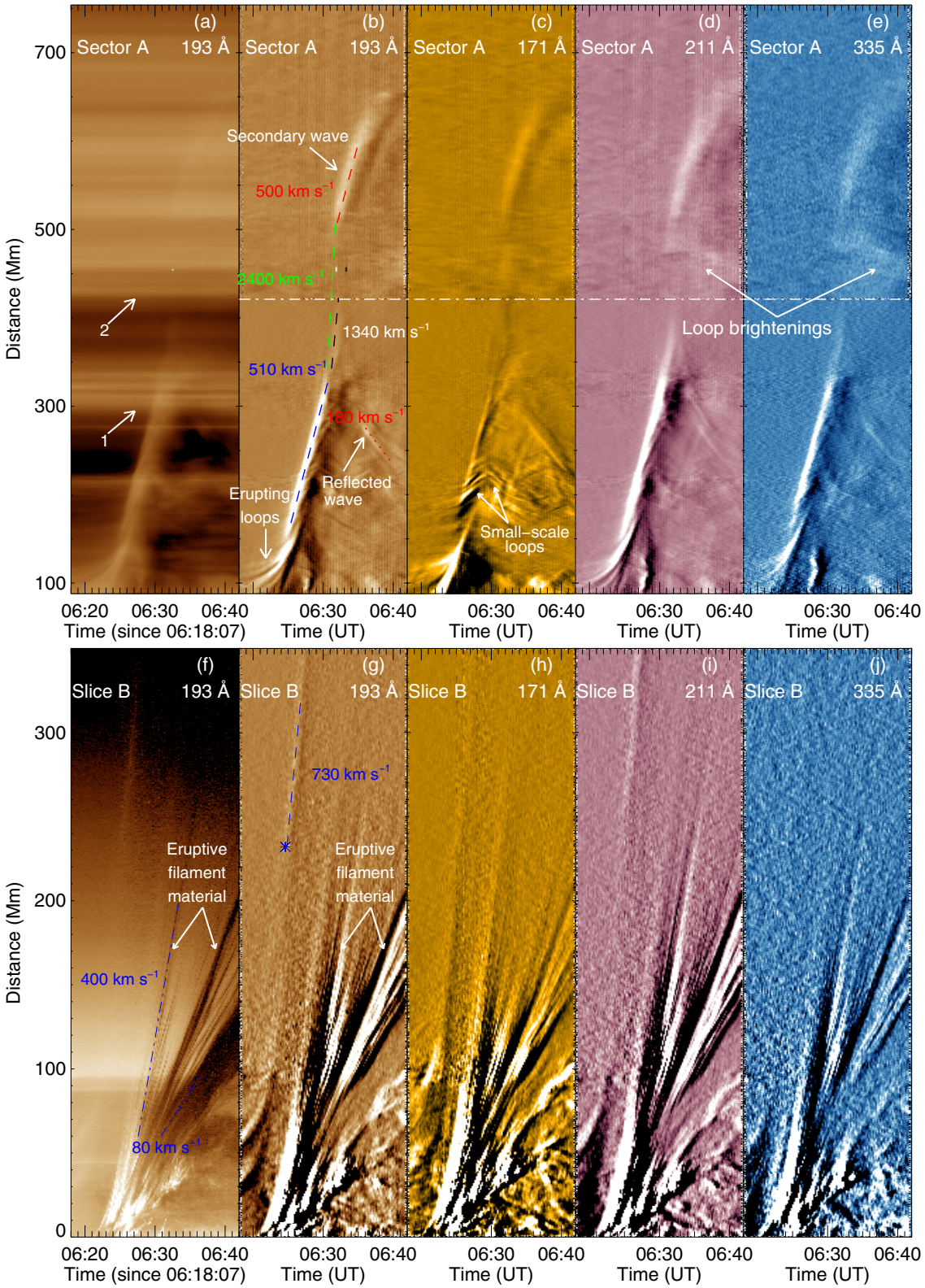

Figure 3. Original and running difference stack plots along Sector "A" and slice "B" at 193, 171, 211, and 335 Å. "1" denotes the coronal bright structure hit by the coronal wave and "2" represents AR 11228. In order to visualize the structures better, the images above and below the dash-dotted line are displayed with different color scales. The asterisk in panel (g) marks the start of the wave dome at the limb.

(A color version of this figure is available in the online journal.)

Figures 3(b)–(e)). In order to investigate the evolution of the reflected wave, we placed Sectors "C"–"E" starting at this structure (Figure 2) and obtained their running difference stack plots as shown in Figure 4. Initially, the reflected wave front propagated at a speed of 140 km s^{-1}. At 06:36:10 UT, another wave front was observed in front of it and propagated at a greater

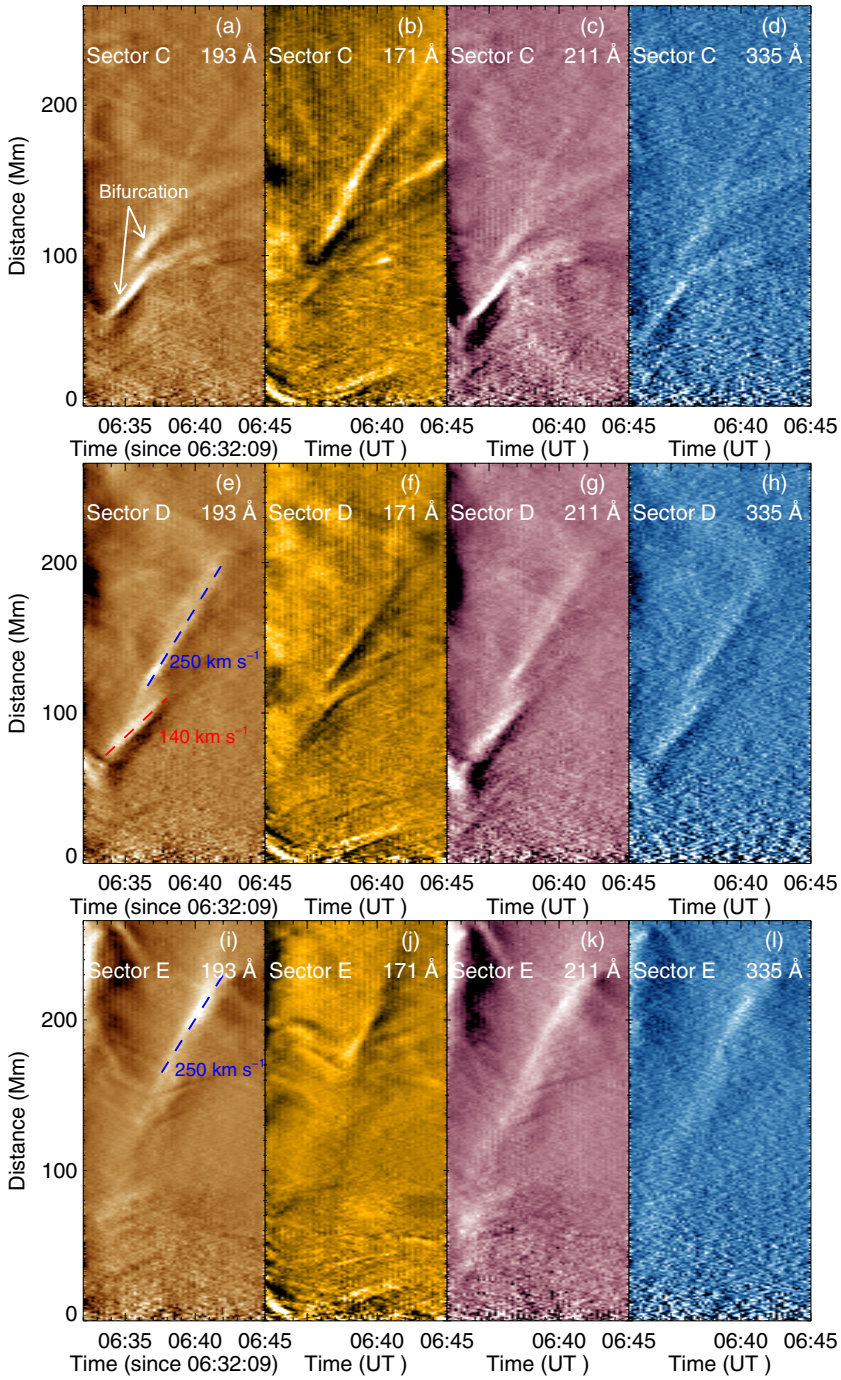

Figure 4. Running difference stack plots at 193, 171, 211, and 335 Å along Sector "C" (top panels), "D" (middle panels), and "E" (bottom panels).
(A color version of this figure is available in the online journal.)

speed of 250 km s^{-1} (Figures 1(f) and 4(e)–(h)). The former and latter wave fronts form a shape of "bifurcation." About 3 minutes later, the former wave front faded below detection. The latter wave front experienced an evident deflection toward the east, and thus the later stage of the wave can be seen in the stack plots of Sectors "D" and "E." Then, the wave disappeared at 06:42:10 UT.

A similar "bifurcation" was also observed when the primary wave approaches the coronal bright structure "3" (Figures 1(a) and (e); see Animation 2). As seen in the stack plot of Sector "F" (Figures 5(a)–(d)), a new wave front initiated in front of it at 06:31:31 UT and propagated at a higher speed ($v \sim 690$ km s^{-1}). This new wave front was subsequently deflected at the boundaries of ARs (see the red segments in Figures 1(d), (f), and (g)), and its propagating direction changed by 71° in 9 minutes, similar to what was observed by Attrill et al. (2007a) and was interpreted as untwisting motions of a twisted flux rope involved in the CME. One hundred seventy-one observations show the wave front in Sector "F" as darkening instead of brightening (Figure 5(b)), similar to that observed by Wills-Davey & Thompson (1999), Liu et al. (2010), Schrijver et al. (2011), and Ma et al. (2011). This is suggestive of heating above the characteristic temperature (0.6 MK) of the 171 Å passband, as simulated by Downs et al. (2011).

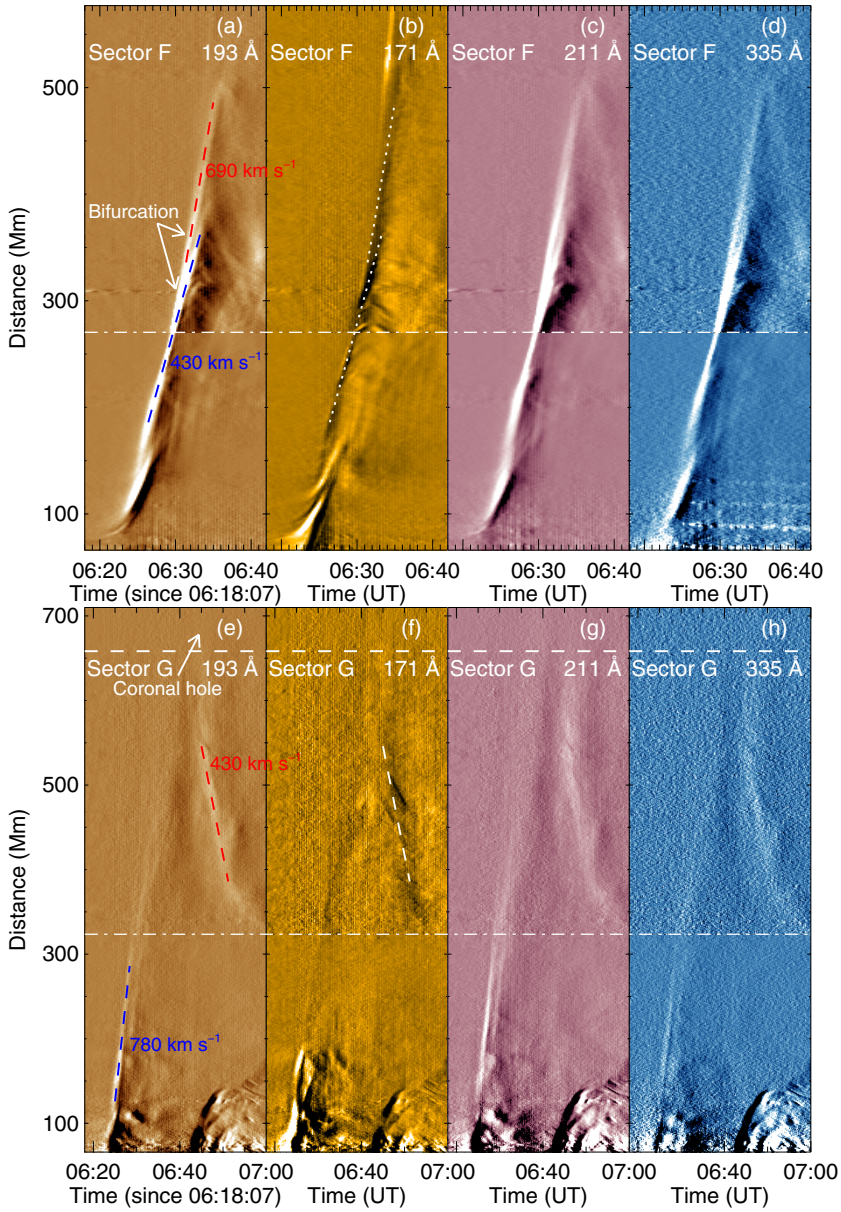

Figure 5. Running difference stack plots at 193, 171, 211, and 335 Å along Sector "F" (top panels) and Sector "G" (bottom panels). In order to visualize the structures better, the images above and below the dash-dotted line are displayed with different color scales. The white dashed line in the bottom panels represents the boundary of the southern polar CH.

(A color version of this figure is available in the online journal.)

Another reflected wave from a southern polar CH (Figure 1(a)) was also observed at 06:46:09 UT (Figures 1(h) and (i)). Seen from the stack plot of Sector "G" (Figures 5(e)–(h)), the primary wave propagated in the southward direction with a speed of about 780 km s^{-1}. The reflected wave from the boundary of the polar CH had a speed ($v \sim 430$ km s^{-1}) lower than that of the primary wave. At 06:51:07 UT, the reflected wave was 320 Mm away from the eruption center, and the velocity decreased to 110 km s^{-1}. The reflected wave from the polar CH at 171 Å appears as emission reduction (Figure 5(f)).

3.4. Three-dimensional Wave Dome

Based on the observed evolution of the wave dome with *SDO* and *STEREO A*, we constructed an approximate three-dimensional shape of the wave dome. The dome is initially assumed to be a spherical crown which is an opaque shell. Then, we adjust the parameters of the spherical crown (radius and height) until the projections seen from the two viewpoints match the observed images. The spherical crowns seen from the *SDO* and *STEREO A* viewpoints are shown in right panels of Figure 6. The height of the spherical crown is nearly 1.5 times as high as its radius (Figures 6(b), (d), and (f)). For example, at 06:25:30 UT, the radius of the spherical crown was approximately 0.34 $R_{\rm sun}$ and the height was 0.51 $R_{\rm sun}$. Its volume was about 3.3% of the solar volume. At 06:28:10 UT, the radius and height increased to 0.45 $R_{\rm sun}$ and 0.675 $R_{\rm sun}$, respectively, resulting in a volume increase of nearly 2.4 times from 06:25:30 UT.

At 06:25:30 UT, the angle between the axis of the dome and the radial direction of eruption center (S22W55) on the surface was about 22° (Figures 6(b) and (d)). About 3 minutes later, the axis of the dome was inclined southward by 15° (Figure 6(f)), and approached the radial direction of eruption center. In fact, the dome-shaped wave front propagates faster in the vertical

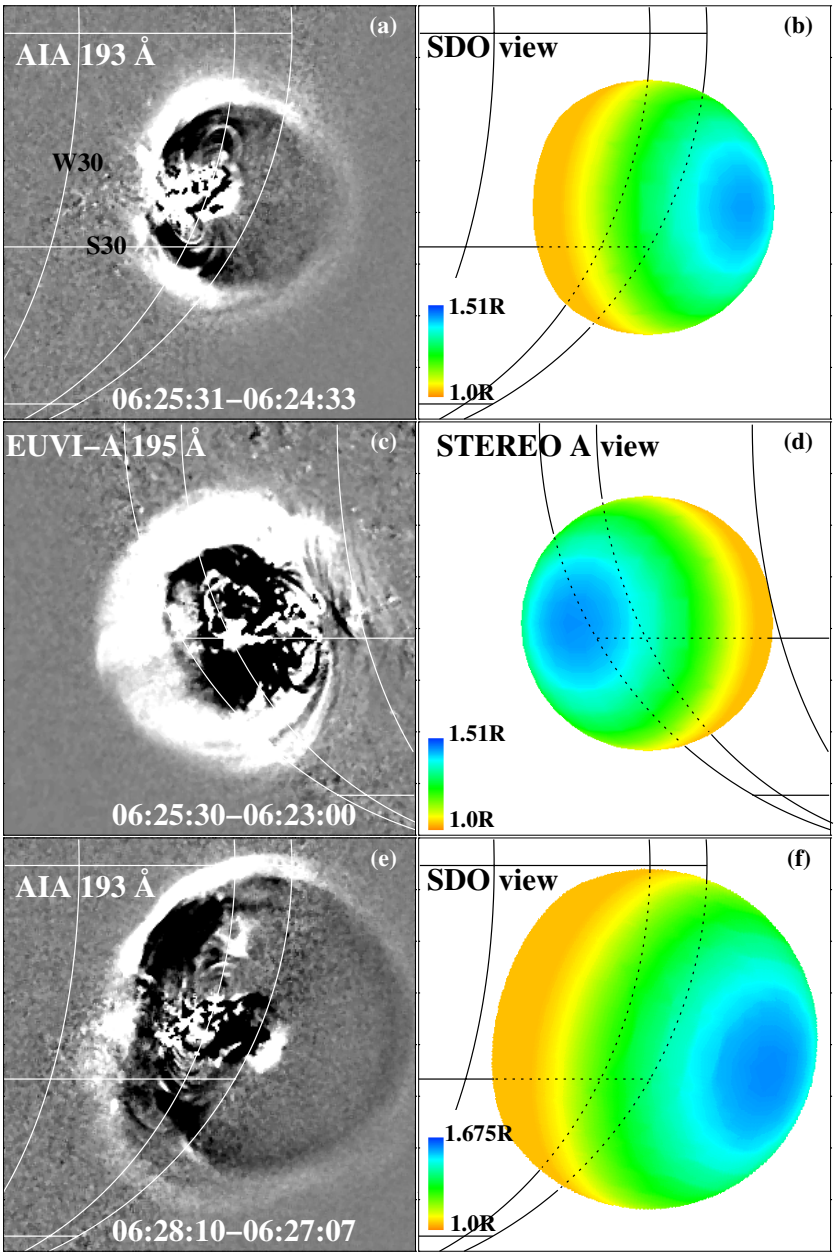

Figure 6. Observed running difference images of AIA 193 Å and EUVI-A 195 Å (left panels) and approximate three-dimensional shape of the wave dome (right panels). Color represents height and "R" denotes the solar radius.

(A color version of this figure is available in the online journal.)

direction than the wave front on the solar surface (Figure 3; Veronig et al. 2010), and the spherical dome evolves gradually into an ellipsoid. Full three-dimensional MHD modeling is required to understand these observations.

4. SUMMARY AND DISCUSSION

The *SDO*/AIA observations of the global coronal EUV wave on 2011 June 7 presented here have revealed several very interesting phenomena.

1. Upon arrival at an AR on its path, the primary EUV wave apparently disappeared and a secondary wave rapidly reemerged within 75 Mm of the AR boundary with a similar speed of 500 km s^{-1}. We speculate two parallel possibilities to explain this discontinuity of wave propagation.

   (a) The AR coronal loops can be perturbed by the impact of the wave and then generate secondary waves, as found in MHD simulations (Ofman & Thompson 2002). In this case, the signal of impact is expected to propagate as a fast-mode wave within the AR. The short duration from the arrival of the primary wave at the AR boundary to the onset of the secondary wave indicates a high velocity of 2400 km s^{-1}, as marked by the green dashed line in Figure 3(b), which is in line with the AR fast-mode speeds found in observations and simulations (Liu et al. 2011; Ofman & Thompson 2002; Williams et al. 2002). However, because the AR has a strong magnetic field and high plasma density, the propagating fast-mode wave could produce very little density, and thus EUV intensity, perturbation, likely

below detection such that the observed wave appears to vanish in the AR.

(b) Another possibility involves the interpretation of the EUV wave as a consequence of field line stretching (e.g., Chen et al. 2002, their Figure 4). In this case, the AR lies below a separatrix surface under overlying, larger-scale loops. When the expanding CME pushes these overlying loops, the short AR loops underneath remain unperturbed, leading to the apparent disappearance of the wave. When the next long field line across the separatrix surface is pushed, a new wave front reappears on the far side of the AR. Because of the short distance between neighboring overlying field lines across the separatrix, this can result in a large apparent velocity of 2400 km s^{-1}.

2. When the EUV wave encounters a bright coronal structure, i.e., small-scale, local loops (instead of large ARs), a new wave front appears there and propagates in front of it at a velocity nearly a factor of two faster (see Figures 4(a)–(h) and 5(a)–(d)). This is somewhat different from recent AIA observations of fast wave fronts overtaking slow ones with a factor of two difference in their speeds (Liu et al. 2010, their Figure 5), but raises similar questions. If the observed wave fronts are indeed MHD waves, their speeds would be determined by the medium in which they propagate. Thus, the speeds along the same direction would be identical, unless the leading wave has altered the local magnetic field and plasma condition, say by compression (Harra et al. 2011), and thus the characteristic wave speed. Our observations suggest that the latter could be the case here. Another possibility is the line of sight projection of waves at different heights. The faster wave front at the bifurcation could result from an upward deflection by the top portion of the small-scale loops toward greater heights, while the slower wave front could be the refraction of the wave at lower heights around these loops. The increase of Alfvén speed and fast-mode speed with height in the low corona within a few solar radius can thus explain their different propagation speeds. Alternatively, this could also be explained if these wave fronts are associated with the expansion of the CME volume of multiple layers at different speeds.
3. There are clearly signatures of reflected waves from a coronal bright structure and a southern polar CH (Figures 3(b)–(e), 4, and 5(e)–(h)). Compared with earlier *STEREO* observations of a similar event on 2007 May 19 (Gopalswamy et al. 2009), AIA's high cadence makes this a stronger case as observational evidence that fast-mode (shock) waves are deflected away from regions of high Alfvén speed and reflected in regions of large Alfvén speed gradients (Uchida et al. 1973; Uchida 1974; Wu et al. 2001; Zhang et al. 2011). In recent MHD simulations, Schmidt & Ofman (2010) suggested that the reflected wave observed by Gopalswamy et al. (2009) was triggered by the magnetic pressure difference between the boundary of the CH and the primary wave, and the excitation of secondary waves in different directions was caused by the induced oscillation of the CH. In this event and the X2.2 flare on 2011 February 15, we find that the reflected waves always propagate fractionally slower than the primary waves, while Gopalswamy et al. (2009) found that the reflected waves in certain directions are faster. In any case, this may suggest that the local plasma condition and thus fast-mode wave speeds are changed upon the passage of the primary wave, as we noted above.
4. We find that the wave has a three-dimensional dome shape, similar to that reported by Veronig et al. (2010). The upward propagation speed of the dome is 730 km s^{-1}, while its lateral expansion speed ranges from 430 to 780 km s^{-1}, depending on the direction (see also Ma et al. 2009). These speeds, a factor of two greater than typical EUV wave speeds of 200–400 km s^{-1} (Klassen et al. 2000; Thompson & Myers 2009), fall in the range of the nonlinear MHD wave/shock category proposed by Warmuth & Mann (2011). In addition, the wave front on the solar surface propagates at nearly constant speeds in front of the expanding loops involved in the CME that accelerates up to 280 km s^{-1}. This is consistent with early *STEREO* results (Kienreich et al. 2009; Patsourakos & Vourlidas 2009), as confirmed with numerical simulations (Cohen et al. 2009). Therefore, our observations suggest that the dome could possibly represent a CME-driven shock front, as recently imaged by AIA (Ma et al. 2011).

In summary, we find a variety of phenomena associated with the interaction of the global EUV wave with local coronal structures, including secondary waves from ARs and small coronal loops (bright structures), as well as reflected waves from CHs and coronal loops. Some of these phenomena can be equally explained by either a wave or a non-wave model alone. However, taken together, these observations provide new evidence for the multitude of global EUV waves, in which a true MHD fast-mode wave/shock propagates in front of an expanding CME bubble (e.g., Zhukov & Auchère 2004; Cohen et al. 2009; Liu et al. 2010; Downs et al. 2011).

We acknowledge SECCHI and AIA for providing data. This work is supported by the National Natural Science Foundations of China (40890161, 11025315, 10921303, and 11003026), the CAS Project KJCX2-YW-T04, the National Basic Research Program of China under grant 2011CB811403, and the Young Researcher Grant of National Astronomical Observatories, Chinese Academy of Sciences. Wei Liu was supported by AIA Contract NNG04EA00C.

REFERENCES

Attrill, G. D. R. 2010, ApJ, 718, 494
Attrill, G. D. R., Harra, L. K., van Driel-Gesztelyi, L., & Démoulin, P. 2007a, ApJ, 656, L101
Attrill, G. D. R., Harra, L. K., van Driel-Gesztelyi, L., Démoulin, P., & Wülser, J.-P. 2007b, Astron. Nachr., 328, 760
Boerner, P., Edwards, C., Lemen, J., et al. 2011, Sol. Phys.
Chen, P. F., Wu, S. T., Shibata, K., & Fang, C. 2002, ApJ, 572, L99
Chen, P. F., & Wu, Y. 2011, ApJ, 732, L20
Cohen, O., Attrill, G. D. R., Manchester, W. B., & Wills-Davey, M. J. 2009, ApJ, 705, 587
Delaboudinière, J.-P., Artzner, G. E., Brunaud, J., et al. 1995, Sol. Phys., 162, 291
Delannée, C. 2000, ApJ, 545, 512
Delannée, C., & Aulanier, G. 1999, Sol. Phys., 190, 107
Downs, C., Roussev, I. I., van der Holst, B., et al. 2011, ApJ, 728, 2
Gallagher, P. T., & Long, D. M. 2011, Space Sci. Rev., 158, 365
Gopalswamy, N., Yashiro, S., Temmer, M., et al. 2009, ApJ, 691, L123
Harra, L. K., Sterling, A. C., Gömöry, P., & Veronig, A. 2011, ApJ, 737, L4
Kaiser, M. L., Kucera, T. A., Davila, J. M., et al. 2008, Space Sci. Rev., 136, 5
Kienreich, I. W., Temmer, M., & Veronig, A. M. 2009, ApJ, 703, L118
Klassen, A., Aurass, H., Mann, G., & Thompson, B. J. 2000, A&AS, 141, 357
Lemen, J. R., Title, A. M., Akin, D. J., et al. 2011, Sol. Phys., 115
Liu, W., Berger, T. E., Title, A. M., & Tarbell, T. D. 2009, ApJ, 707, L37

Liu, W., Nitta, N. V., Schrijver, C. J., et al. 2010, ApJ, 723, L53
Liu, W., Title, A. M., Zhao, J., et al. 2011, ApJ, 736, L13
Ma, S., Raymond, J. C., Golub, L., et al. 2011, ApJ, 738, 160
Ma, S., Wills-Davey, M. J., Lin, J., et al. 2009, ApJ, 707, 503
Moses, D., Clette, F., Delaboudinire, J.-P., et al. 1997, Sol. Phys., 175, 571
O'Dwyer, B., Del Zanna, G., Mason, H. E., Weber, M. A., & Tripathi, D. 2010, A&A, 521, A21
Ofman, L., & Thompson, B. J. 2002, ApJ, 574, 440
Patsourakos, S., & Vourlidas, A. 2009, ApJ, 700, L182
Podladchikova, O., & Berghmans, D. 2005, Sol. Phys., 228, 265
Schmidt, J. M., & Ofman, L. 2010, ApJ, 713, 1008
Schrijver, C. J., Aulanier, G., Title, A. M., Pariat, E., & Delannee, C. 2011, ApJ, 738, 167
Schwer, K., Lilly, R. B., Thompson, B. J., & Brewer, D. A. 2002, AGU Fall Meeting Abstracts, abstract #SH21C-01
Thompson, B. J., Gurman, J. B., Neupert, W. M., et al. 1999, ApJ, 517, L151
Thompson, B. J., & Myers, D. C. 2009, ApJS, 183, 225
Thompson, B. J., Plunkett, S. P., Gurman, J. B., et al. 1998, Geophys. Res. Lett., 25, 2465
Uchida, Y. 1974, Sol. Phys., 39, 431
Uchida, Y., Altschuler, M. D., & Newkirk, G., Jr. 1973, Sol. Phys., 28, 495
Veronig, A. M., Muhr, N., Kienreich, I. W., et al. 2010, ApJ, 716, L57
Veronig, A. M., Temmer, M., Vršnak, B., & Thalmann, J. K. 2006, ApJ, 647, 1466
Vršnak, B., & Cliver, E. W. 2008, Sol. Phys., 253, 215
Wang, Y.-M. 2000, ApJ, 543, L89
Warmuth, A., & Mann, G. 2011, A&A, 532, A151
Warmuth, A., Vršnak, B., Aurass, H., & Hanslmeier, A. 2001, ApJ, 560, L105
Williams, D. R., Mathioudakis, M., Gallagher, P. T., et al. 2002, MNRAS, 336, 747
Wills-Davey, M. J., & Attrill, G. D. R. 2009, Space Sci. Rev., 149, 325
Wills-Davey, M. J., & Thompson, B. J. 1999, Sol. Phys., 190, 467
Wu, S. T., Zheng, H., Wang, S., et al. 2001, J. Geophys. Res., 106, 25089
Wuelser, J. P., Lemen, J. R., Tarbell, T. D., et al. 2004, Proc. SPIE, 5171, 111
Zhang, Y., Kitai, R., Narukage, N., et al. 2011, PASJ, 63, 685
Zhukov, A. N. 2011, J. Atmos. Sol.-Terr. Phys., 73, 1096
Zhukov, A. N., & Auchère, F. 2004, A&A, 427, 705